RESEARCH OF DYNAMIC PROCESSES IN A LAYER
DURING COLLISION WITH AN IMPACTOR

Yuriy PYR'YEV*, Marek PAWLIKOWSKI**, Rafał DROBNICKI**, Andrzej PENKUL***

* Faculty of Mechanical and Industrial Engineering, Institute of Mechanics and Printing, Department of Printing Technologies,
Warsaw University of Technology, Konwiktorska 2, 00-217 Warsaw, Poland
** Faculty of Mechanical and Industrial Engineering, Institute of Mechanics and Printing, Department of Construction Engineering and Biomedical
Engineering, Warsaw University of Technology, Narbutta 85, 02-524 Warsaw, Poland
*** Faculty of Mechanical and Industrial Engineering, Institute of Mechanics and Printing, Department of Mechanics and Weaponry Technology,
Warsaw University of Technology, Narbutta 85, 02-524 Warsaw, Poland

yuriy.pyryev@pw.edu.pl, marek.pawlikowski@pw.edu.pl, rafal.drobnicki@pw.edu.pl , andrzej.penkul@pw.edu.pl

Abstract: The article concerns the modeling of the transverse impact of an impactor (test sample) on the surface of an infinite elastic layer. The Laplace transform with respect to time and the Hankel transform with respect to the radius for the axisymmetric case were applied. The propagation of elastic waves in the layer and local deformations in the contact zone are taken into account. Impact force, impact time and the coefficient of restitution were examined. The results are compared with the elastic half-space. The calculations carried out showed that for layer thicknesses of more than five impactor diameters, the layer can be considered as a half-space.

Key words: collision, impactor, anvil, elastic layer, plate, Hertz's theory, elastic waves, impact speed, integral transforms

1. INTRODUCTION

The purpose of the paper is to analyse the wave phenomena occurring during the impact of an impactor (rod, test sample) against an anvil (elastic layer) and to develop a method for calculating the parameters of selected physical quantities occurring in the anvil and impactor in the initial post-impact period. The paper continues the analysis of modelling of the anvil considered in [1] as an elastic half-space.

Many examples of impact-type transient processes with different strain rates can be found in the fields of seismology, earthquake engineering, dynamic soil-substrate interactions and terrain characterization, aviation, machinery, transportation, civil engineering, agriculture, military applications, mathematical modeling of erosion processes, spraying [2-11].

A study of the transient waves generated in the layer by the application of a normal linear and point load with rapid changes in time was carried out in papers [7, 10, 12-14]. The Laplace transform with respect to time and the exponential Fourier transform with respect to the longitudinal variable for the linear load and the Hankel transform due to the radius for the axisymmetric case were applied.

The infinite plate model was formulated in papers [15, 16] as a closed form approximation for the initial elastic impact response of an isotropic plate. In paper [17] an analytical solution of the Zener equation was proposed to predict elastic impact of a sphere on the large plate. Energy loss caused by bending wave and motions of the sphere and the plate were studied utilising contact force history.

It was later extended to orthotropic plates [18, 19], which was used to study the elastic impact of orthotropic composite laminates. In the paper [20], plastic deformation and bending vibrations were taken into account for such a model, a non-linear elastic-plastic model was presented to evaluate the coefficient of restitution R_f.

In paper [21] the authors replaced the nonlinear contact law with the linear one to solve Zener model for elastic sphere impacts on large, thin plates. They cocnluded that the solution well agree for $\lambda^* < 0.85$ and $R_f^* > 0.2$ (defined in section 3.2). Such a linearisation method was utilised to investigate the cotact time [22] and the energy sissipation [23]. The effect of elastic waves on elastoplastic strain was studied in [24].

The problem of collision of elastic bodies in terms of their deformation has a rich history. Elementary collision theory uses the coefficient of restitution R_f as the key parameter to characterise the deformation properties of colliding bodies and does not reflect the various characteristics of the internal state of bodies [5, 25].

In practice, the Hertzian impact theory is used to determine the stresses occurring during the interaction of two bodies [6].

Sears [26] considered the influence of the spherical shape of the rod ends on the obtained results. In these studies, he took into account both local deformations and wave propagation. This approach led to a good agreement of theoretical and experimental results and is used in many subsequent works [27, 28].

The theory of crossbeam impact comes from Timoshenko [29].

Paper [7] presents an overview of the approaches developed by the author and his colleagues to study the effect of a blunted elastic body on the surface of an elastic medium. Mathematically, the problem is generally formulated as a non-stationary mixed boundary problem of continuum mechanics, in which the unknown contact limit varies in time and space. The process of collision between a blunt body and an elastic medium always involves a supersonic phase, during which the boundary value problem can

sciendo

Yuriy Pyr'yev, Marek Pawlikowski, Rafał Drobnicki, Andrzej Penkul
Research of Dynamic Processes in a Layer During Collision with an Impactor

DOI 10.2478/ama-2024-0062

be formulated as a non-mixed boundary and thus solved by simpler methods [7, 8, 30].

The impact of the supersseismic phase on the collision process immediately after the first contact is investigated within the framework of Hertz's theory of impacts in [30]. For small values of the α_A parameter (defined in point 4), the influence of the supersseismic state on the course of the impact can be neglected.

Paper [31] presents a numerical analysis of the plastic target plate behaviour evoked by the high-velocity impact of a blunt-nosed cylindrical rigid projectile. The impact strength of elastic bars of variable cross-section was nalysed in [32] to investigate the relation between the restitution coefficient and the imacting body shape.

We will consider the collision of an impactor with an elastic layer. The study will be carried out under the basic geometrical assumptions of Hertzian theory [33]

We limit ourselves to considering the direct interaction of the central bodies, i.e. we assume that they are the resultant of the dynamic contact pressures applied to the colliding bodies, directed along a straight line connecting their centers of inertia and coinciding with the normal to the compression surface at the point of initial contact of the non-deformed the surface of these bodies.

This simplifying assumption will allow us to consider only one component of the displacement of bodies at a point coinciding with their point of initial contact.

2. IMPACT PROBLEM STATEMENT

Assuming that a heavy body strikes an elastic layer and, at the moment of contact, a layer of thickness h has a velocity of V_0. Under impact, local deformations will occur in the elastic layer and in an impact cylinder of radius r_0, and, in addition, vibrations of the layer are produced. We assume that the friction between the contacting surfaces is negligible and that the elastic layer material with Young's modulus E and Poisson's ratio ν does not undergo plastic deformation or cracking.

The assumption of elastic behaviour of the metal layer (anvil) can be extended to the case of real processes where there is only local plastic deformation in the material, limited by the proximity of the initial point of contact; moreover, the energy required to produce a residual indentation is only a small fraction of the initial kinetic energy [34].

Continuing with the contact between the impactor and the layer, the displacements of the impactor will consist of a part dependent on the local compression and a part determined by the dynamic deflections of the layer. As is known, the dynamic deflections of the layer satisfy the differential equations [10].

2.1. Mathematical model of the elastic layer

A point source gives rise to volumetric longitudinal (P) and shear (S) waves, Rayleigh-Lamb waves and Rayleigh (R) waves. In [35], Lamb considered the problems of wave propagation in an isotropic elastic layer.

Let us consider in a cylindrical coordinate system (r, θ, z) a layer $(0 \leq z < h)$, where r – radial and z – axial coordinates; θ – angular coordinate (Fig. 1). The medium is assumed to be homogeneous and isotropic. Axially symmetric non-stationary loads depending on position and time act on the surface $p(r, t)$ with relative spatial distribution $Z(r)$ and the resultant $P(t)$; i.e.

$p(r, t) = Z(r)P(t)$ in time $t > 0$. As a result of this action, there is a vector field of displacement in the structure $U \equiv (u, 0, w)$, where u, w are the components of the displacement vector on the axis, r, z respectively.

An elastic layer is characterized by the velocities of longitudinal (P) c_1 and shear (S) c_2 waves or the Lame constants λ, μ, and density ρ, which are related by $c_1=((\lambda+2\mu)/\rho)^{1/2}$, $c_2=(\mu/\rho)^{1/2}$.

On the free surface of the medium, stresses $\sigma_{zr}, \sigma_{z\theta}, \sigma_{zz}$ are either converted to zero or take values corresponding to a given limit load.

We assume that the medium is at rest and at the initial moment $t = 0$ the axisymmetric disturbance source starts to act $p(r, t)=Z(r)P(t)$.

As a rule, the forces arising during an impact $P(t)$ (impact force) are not known in advance, they must be determined in the problem-solving process, and only in some cases can they be considered predetermined.

The discussed issue boils down to solving Lamé displacement equations in a cylindrical coordinate system [10, 12]:
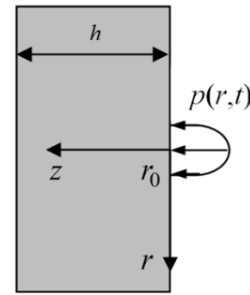
Fig. 1. Physical model of an anvil (elastic layer) with a surface area load with r_0 radius

$$(\lambda + 2\mu)\left(\frac{\partial^2 u}{\partial r^2} + \frac{1}{r}\frac{\partial u}{\partial r} - \frac{u}{r^2}\right) + \mu\frac{\partial^2 u}{\partial z^2} + (\lambda + \mu)\frac{\partial^2 w}{\partial r\,\partial z} = \rho\frac{\partial^2 u}{\partial t^2},$$
$$(\lambda + \mu)\left(\frac{\partial^2 u}{\partial r\,\partial z} + \frac{1}{r}\frac{\partial u}{\partial r}\right) + \mu\left(\frac{\partial^2 w}{\partial r^2} + \frac{1}{r}\frac{\partial w}{\partial r}\right) + (\lambda + 2\mu)\frac{\partial^2 w}{\partial z^2} = \rho\frac{\partial^2 w}{\partial t^2},$$
$$0 \leq r < \infty,\ 0 \leq z \leq h,\ t \geq 0 \tag{1}$$

at boundary conditions:

$$\sigma_{zz}(r, 0, t) = -p(r, t) = -Z(r)P(t), 0 \leq r < \infty,\, t \geq 0 \tag{2}$$

$$\sigma_{rz}(r, 0, t) = 0,\ 0 \leq r < \infty,\, t \geq 0 \tag{3}$$

$$\sigma_{zz}(r, h, t) = 0,\ \sigma_{rz}(r, h, t) = 0,\ 0 \leq r < \infty,\, t \geq 0 \tag{4}$$

and the initial conditions $t = 0$ [10]:

$$u = 0,\ \frac{\partial u}{\partial t} = 0,\ w = 0,\ \frac{\partial w}{\partial t} = 0,\ 0 \leq r < \infty, 0 \leq z \leq h \tag{5}$$

$p(r, t)$ is the contact pressure distributed over the contact area $\omega(t)$. Due to the axis of symmetry, $\omega(t)$ is a circle with a radius $a(t)$. We assume that the contact area does not change with time and from the beginning the radius is equal to r_0.

We will consider the sources $Z(r)$ on the surface for which the following condition is met

$$2\pi \int_0^\infty Z(r)P(t)r\,dr = P(t), \tag{6}$$

where [6]

$$Z(r) = \frac{1}{\pi r_0^2}\frac{3}{2}\sqrt{\left(1 - \frac{r^2}{r_0^2}\right)}H\left(1 - \frac{r^2}{r_0^2}\right). \tag{7}$$

where $H(t)$ Heaviside function: $H(t) = 0$ for $t < 0$, $H(t) = 1$ for $t \geq 0$.

For comparison, we will model the anvil as an elastic plate. In this analysis of the response of large plates to localised impulse forces, we will use the usual approximate theory of thin plates. This theory assumes that the radius of curvature of the plate is everywhere large compared to its thickness, and that the angle between the plate and the original plane is everywhere small. From this approximate theory it follows that the displacement $w^*(0,t)$ of the point of application is proportional to the impulse $P(t)$ [15]

$$w^* = \alpha^* \int_0^t P(t')\,dt' \qquad (8)$$

with

$$\alpha^* = \sqrt{\frac{3\rho(1-v^2)}{E}}\,\frac{1}{16\rho(h^*)^2}\,,$$

where h^* is the half-thickness of the plate. The displacement w^* refers strictly to the displacement of the centre plane of the plate.

2.2. Mathematical model of the impactor hitting the layer

In the study of the response of the layer to impact, the system of equations describing the behaviour of waves in the layer integrates simultaneously with the equation of motion of the impactor and the condition of compliance of displacements. The last one takes into account a contact approximation of a sample with mass m_1 and layer. One of the ends of the cylindrical rod is hemispherical. We will consider that for the considered impact of the impactor, the contact approximation can be determined based on the solution to the dynamic problem of Hertz for pressing a ball into an elastic half-space [6].

Let us denote, after S.P. Timoshenko [29], the total displacement of the hitting body (impactor) from the start of the impact as $W(t)$, and local compression as α_H. Then, of course [19, 29]

$$W = \alpha_H + w \qquad (9)$$

where $w = w(0, 0, t)$ deflection of the elastic layer surface under the impactor. The displacement $W(t)$ satisfies the differential equation of motion

$$m_1 \frac{d^2 W(t)}{dt^2} = -P(t) \qquad (10)$$

under initial conditions:

$$W(0) = 0, \frac{dW}{dt} = V_0,\ t = 0 \qquad (11)$$

here $P(t)$ is the resultant of the contact pressure.
In the following part, we assume that

$$\frac{m_1}{P}\frac{\partial^2 w_e}{\partial t^2} \ll 1 \qquad (12)$$

where $w_e(r, z, t)$ characterizes the relative displacement of the sample elements due to its deformation.

3. SOLUTION METHOD

3.1. Key dependencies for the flexible layer

In this article, the approach [10] was used to find the stress-strain state of an elastic layer with a thickness h. Applying the Laplace and Hankel transformations to equations (1) and taking

into account uniform initial conditions (5), we obtain linear differential equations with respect to the variable z. Since the solution to these equations depends on four unknowns, they can be found using the four boundary conditions (2)-(4). Using the inverse Laplace and Hankel transformations, we obtain the desired relationships. The displacements u, w and stresses can be expressed by the Duhamel integral

$$\{u(r,z,t), w(r,z,t)\} = \int_0^t \{u_\delta(r,z,t-t'), w_\delta(r,z,t-t')\} \cdot P(t')dt' = \{u_\delta(r,z,t), w_\delta(r,z,t)\} * P(t) \qquad (13)$$

$$\{\sigma_{zz}, \sigma_{rr}, \sigma_{\theta\theta}, \sigma_{rz}\} = \{\sigma_{zz,\delta}, \sigma_{rr,\delta}, \sigma_{\theta\theta,\delta}, \sigma_{rz,\delta}\} * P(t) \qquad (14)$$

where $u_\delta(r,z,t)$, $w_\delta(r,z,t)$ are solutions to problem (1)-(6) for the impulse function $P(t) = \delta(t)$: $\delta(t) = \infty$ for $t = 0$, $\delta(t) = 0$ for $t \neq 0$ and

$$\int_{-\infty}^{+\infty} \delta(t)dt = 1\,. \qquad (15)$$

Applying the Laplace and Hankel integral transformations to the considered problem (1) - (6) [10] e.g. for displacement $w_\delta(r,z,t)$

$$w_\delta^L(r,z,s) = \int_0^\infty w_\delta(r,z,t)e^{-st}dt \qquad (16)$$

$$w_\delta^{LH}(k,z,s) = \int_0^\infty w_\delta^L(r,z,s)rJ_0(kr)dr \qquad (17)$$

we get a solution to the problem of the following form [36]:

$$\{u_\delta, w_\delta\} = \frac{1}{2\pi i}\int_{c_0-i\infty}^{c_0+i\infty}\{u_\delta^L, w_\delta^L\}e^{st}ds \qquad (18)$$

$$\{\sigma_{zz,\delta}, \sigma_{rr,\delta}, \sigma_{rz,\delta}\} = \frac{1}{2\pi i}\int_{c_0-i\infty}^{c_0+i\infty}\{\sigma_{zz,\delta}^L, \sigma_{rr,\delta}^L, \sigma_{rz,\delta}^L\}e^{st}ds \qquad (19)$$

where:

$$\{w_\delta^L, \sigma_{zz,\delta}^L\} = \int_0^\infty\{w_\delta^{LH}, \sigma_{zz,\delta}^{LH}\}Z^H(k)kJ_0(kr)dk \qquad (20)$$

$$\{u_\delta^L, \sigma_{rz,\delta}^L\} = \int_0^\infty\{u_\delta^{LH}, \sigma_{rz,\delta}^{LH}\}Z^H(k)kJ_1(kr)dk \qquad (21)$$

$$\sigma_{rr,\delta}^L = \int_0^\infty \sigma_{rr,\delta}^{LH0}Z^H kJ_0(kr)dk + \frac{1}{r}\int_0^\infty \sigma_{rr,\delta}^{LH1}Z^H kJ_1(kr)dk \qquad (22)$$

$J_n(kr)$ is a Bessel function of the first kind of order n ($n = 0, 1, \dots$), k is positive parameter, c_0 is a real number so that the contour path of integration is in the region of convergence of $u_\delta{}^{LH}(k,z,s)$, $w_\delta{}^{LH}(k,z,s)$.

Integral expressions in (18)-(22) marked with "LH" have the following form

$$u_\delta^{LH}(k,z,s) = -(D_1 k\,\mathrm{ch}(\alpha_1 z) + D_2 k\,\frac{\mathrm{sh}(\alpha_1 z)}{\alpha_1} + D_3\,\alpha_2^2\,\frac{\mathrm{sh}(\alpha_2 z)}{\alpha_2} + D_4\,\mathrm{ch}(\alpha_2 z)) \qquad (23)$$

$$w_\delta^{LH}(k,z,s) = (D_1\alpha_1^2\,\frac{\mathrm{sh}(\alpha_1 z)}{\alpha_1} + D_2\mathrm{ch}(\alpha_1 z) + D_3 k\,\mathrm{ch}(\alpha_2 z) + D_4 k\,\frac{\mathrm{sh}(\alpha_2 z)}{\alpha_2}) \qquad (24)$$

$$\sigma_{zz,\delta}^{LH}(k,z,s) = \mu(D_1\gamma\,\mathrm{ch}(\alpha_1 z) + D_2\gamma\,\frac{\mathrm{sh}(\alpha_1 z)}{\alpha_1} + D_3 2k\alpha_2^2\,\frac{\mathrm{sh}(\alpha_2 z)}{\alpha_2} + D_4\,2k\mathrm{ch}(\alpha_2 z))\,, \qquad (25)$$

$$\sigma_{rz,\delta}^{LH}(k,z,s) = -\mu(D_1 2k\alpha_1^2\,\frac{\mathrm{sh}(\alpha_1 z)}{\alpha_1} + D_2 2k\,\mathrm{ch}(\alpha_1 z) + D_3\gamma\,\mathrm{ch}(\alpha_2 z) + D_4\,\gamma\frac{\mathrm{sh}(\alpha_2 z)}{\alpha_2})\,, \qquad (26)$$

$$\sigma_{rr,\delta}^{LH0}(k,z,s) = -(D_1(k^2(\lambda + 2\mu) - \alpha_1^2\lambda)\mathrm{ch}(\alpha_1 z) + D_2(k^2(\lambda + 2\mu) - \alpha_1^2\lambda)\,\frac{\mathrm{sh}(\alpha_1 z)}{\alpha_1} + 2D_3 k\alpha_2^2\,\mu\,\frac{\mathrm{sh}(\alpha_2 z)}{\alpha_2} + D_4 2k\mu\,\mathrm{ch}(\alpha_2 z)) \qquad (27)$$

$$\sigma_{rr,\delta}^{LH1}(k,z,s) = 2\mu(D_1 k\mathrm{ch}(\alpha_1 z) + D_2 k\,\frac{\mathrm{sh}(\alpha_1 z)}{\alpha_1} + D_3\alpha_2^2\,\frac{\mathrm{sh}(\alpha_2 z)}{\alpha_2} + D_4\,\mathrm{ch}(\alpha_2 z))\,, \qquad (28)$$

Yuriy Pyr'yev, Marek Pawlikowski, Rafał Drobnicki, Andrzej Penkul
Research of Dynamic Processes in a Layer During Collision with an Impactor

DOI 10.2478/ama-2024-0062

$$\sigma_{\theta\theta,\delta}^{LH0}(k,z,s) = \lambda a^2 s^2 \left(D_1 \text{ch}(\alpha_1 z) + D_2 \frac{\text{sh}(\alpha_1 z)}{\alpha_1}\right) \qquad (29)$$

$$\sigma_{\theta\theta,\delta}^{LH1}(k,z,s) = -2\mu\left(D_1 k\,\text{ch}(\alpha_1 z) + D_2 k \frac{\text{sh}(\alpha_1 z)}{\alpha_1} + \right.$$

$$\left. D_3 \alpha_2^2 \frac{\text{sh}(\alpha_2 z)}{\alpha_2} + D_4 \text{ch}(\alpha_2 z)\right),$$

$$D_1 = -Z^H \gamma (8k^2(1 - C_1 C_2) + 2\gamma^2 S_1 S_2)/D,$$

$$D_2 = -Z^H 2\gamma (4k^2 \alpha_1^2 S_1 C_2 - \gamma^2 C_1 S_2)/D,$$

$$D_3 = Z^H 4k (4k^2 \alpha_1^2 S_1 C_2 - \gamma^2 C_1 S_2)/D,$$

$$D_4 = -Z^H 4k (\gamma^2 (1 - C_1 C_2) + 4k^2 \alpha_1^2 \alpha_2^2 S_1 S_2)/D,$$

$$D(k,s) = 2\mu\{8k^2 \gamma^2 (1 - C_1 C_2) + (\gamma^4 + (4k^2 \alpha_1 \alpha_2)^2) S_1 S_2\},$$

$$\gamma = 2k^2 + c_2^{-2} s^2, \qquad (30)$$

$$C_j = \text{ch}(h\alpha_j),\ S_j = \frac{\text{sh}(h\alpha_j)}{\alpha_j},\ \alpha_j = \sqrt{k^2 + c_j^{-2} s^2},\ j = 1,2 \qquad (31)$$

Hankel transform $Z^H(k)$ of the $Z(r)$ source on the surface (7)

$$Z^H(k) = \frac{3(\sin(r_0 k) - r_0 k \cos(r_0 k))}{2\pi r_0^3 k^3} \qquad (32)$$

Analysis of the elements of the characteristic equation $D(k, s)=0$ was carried out for example in [37].

In order to receive the function $w_\delta(0,0,t)$ for the initial moment $t \to 0$ we find the properties of the Laplace transform for $s \to \infty$

$$w_\delta^{LH}(k,z,s) = \frac{c_2^2 e^{-\frac{zs}{c_1}}}{\mu c_1}\left(\frac{1}{s} - \frac{c_1 z k^2}{2s^2} + \cdots\right) - \frac{2c_2^4 k^2 e^{-\frac{zs}{c_2}}}{\mu c_1 s^3}. \qquad (33)$$

In the initial moment we get

$$w_\delta(0,0,t) = \frac{c_2^2}{\mu c_1} H(t) Z(0),\ t \to 0 \qquad (34)$$

$$\sigma_{zz,\delta}(0,z,t) = -\delta(t - z/c_1) Z(0),\ t - z/c_1 \to 0 \qquad (35)$$

Asymptotics (35) shows that for the calculation of stresses it is better to use

$$\sigma_{zz}(r,z,t) = \int_0^t \sigma_{zz,H}(r,z,t-t') \frac{d}{dt'} P(t') dt' \qquad (36)$$

where $\sigma_{zz,H}(k,z,s) = \sigma_{zz,\delta}(k,z,s)/s$.

The calculations of the inverse integral Laplace and Hankel transformations were performed in the same way as in the papers [36,38].

3.2. Solution method for the impactor

Integrating the equation (10) using the Laplace transform and the initial conditions (11), we obtain

$$W(t) = V_0 t - \frac{1}{m_1} \int_0^t (t - t') P(t') dt' \qquad (37)$$

On the other hand, according to the theory of Hertz [6], we can assume

$$\alpha_H = (P/K)^{2/3} = k_0 P^{2/3}\ \text{or}\ P = K\alpha_H^{3/2} \qquad (38)$$

where K is determined from the equation [6]

$$K = \frac{4E^*\sqrt{r_0}}{3},\ k_0 = K^{-2/3},\ \frac{1}{E^*} = \frac{1-v_1^2}{E_1} + \frac{1-v^2}{E} \qquad (39)$$

Taking (9), (37), (38) into account, we obtain the equation

$$V_0 t - \frac{1}{m_1} \int_0^t (t - t') P(t') dt' = k_0 P(t)^{2/3} + w(0,0,t) \qquad (40)$$

At the moment of time $t = t_n = n\Delta t$, $n = 0, 1, 2, \ldots$, Δt integration time is assumed to take place

$$V_0 t_n - \frac{1}{m_1} \int_0^{t_n}(t_n - t') P(t') dt' = k_0 P(t_n)^{2/3} + w_n \qquad (41)$$

where $w_n = w(0,0,t_{n-1})$.

In the initial moment $t = 0$ ($n = 0$), sample displacement $W = 0$, displacement of half-space $w = 0$, sample speed $v = V_0$.

In moment $t = t_1$ ($n = 1$), sample displacement $W(t_1) = W_1 = V_0 t_1$, deflection of half-space $w(0,0,t_0) = w_1 = 0$, impact force (pressure) $P(t_1) = P_1 = K(W_1 - w_1)^{3/2}$, acceleration of the sample $a_1 = -P_1/m_1$, sample speed $v(t_1) = v_1 = V_0$.

In the time moment $t = t_2$ ($n = 2$), sample displacement $W(t_2) = W_2 = W_1 + v_1 \Delta t + a_1 (\Delta t)^2/2$, deflection of layer $w(0,0,t_1) = w_2$, impact force (pressure) $P(t_2) = P_2 = K(W_2 - w_2)^{3/2}$, acceleration of the sample $a_2 = -P_2/m_1$, sample speed $v(t_2) = v_2 = v_1 + a_1 \Delta t$.

The further course of the calculations is obvious. Let us write directly the formulas related to the nth stage:

$$W(t_n) = W_n = W_{n-1} + v_{n-1}\Delta t + a_{n-1}(\Delta t)^2/2 \qquad (42)$$

$$w_n = \Delta t \sum_{m=1}^{n-2} w_\delta(0,0,t_{n-1}-t_m) P_m + \frac{\Delta t}{2} w_\delta(0,0,0) P_{n-1} \qquad (43)$$

$$P(t_n) = P_n = K(W_n - w_n)^{3/2} \qquad (44)$$

$$a_n = -P_n/m_1 \qquad (45)$$

$$v(t_n) = v_n = v_{n-1} + a_{n-1}\Delta t \qquad (46)$$

For the impactor impact issue with a 2h* thick plate, the contact condition will be [19, 29]

$$W = \alpha_H + w^* \qquad (47)$$

We can therefore obtain a single equation for only one dependent variable α_H by differentiating equation (8) twice with respect to time and then subtracting this equation from equation (10). Taking into account condition (47), the following equation is obtained [15]:

$$\frac{d^2\alpha_H}{dt^2} + \frac{1}{m_1} P(\alpha_H) + \alpha^* \frac{d}{dt} P(\alpha_H) = 0 \qquad (48)$$

The non-linear differential equation proposed by Zener [15] is transformed to provide a solution by simplifying the Hertzian force P as a function of local compression α_H. Thus, equation (48) is rewritten as

$$\frac{d^2\alpha_H}{dt^2} + \frac{1}{m_1} K\alpha_H^{3/2} + \frac{3}{2}\alpha^* K\alpha_H^{1/2}\frac{d\alpha_H}{dt} = 0 \qquad (49)$$

under initial conditions:

$$\alpha_H(0) = 0, \frac{d\alpha_H}{dt} = V_0,\ t = 0 \qquad (50)$$

A problem formulated in this way can be transformed into a dimensionless form

$$\frac{d^2\alpha}{d\tau^2} + \alpha^{3/2} + \frac{3}{2}\lambda^*\alpha^{1/2}\frac{d\alpha}{d\tau} = 0 \qquad (51)$$

under initial conditions:

$$\alpha(0) = 0, \frac{d\alpha}{d\tau} = 1,\ \tau = 0 \qquad (52)$$

where $\alpha = \alpha_H/(TV_0)$, $\tau = t/T$, $T = (m_1)^{2/5} V_0^{-1/5} K^{-2/5}$.

$$\lambda^* = \alpha^* K V_0^{1/2} T^{3/2}. \qquad (53)$$

By solving the problem (51), (52) the semi-imperial formula for the coefficient of restitution was derived R_f^* [15] as a function of inelasticity parametr λ^*

$$R_f^* = \exp\left(-1.7191\lambda^*\right). \tag{54}$$

4. NUMERICAL RESULTS

A numerical analysis of the collision of a copper test sample with a steel anvil was carried out [1]. The parameters are given in Tab. 1. The mass of the tested sample m_1 = 0.0122 kg, sample radius r_0 = 0.004 m, collision speed V_0 = 10 m s^{-1} i V_0 = 100 m s^{-1}.

For the problem under consideration [39], the $\alpha_A = (\pi\rho r_0^3/m_1)^{1/2}(V_0/c_1)^{3/2} = 0.785\cdot10^{-3}$ parameter was calculated. Due to the low value of α_A, the influence of the super-seismic state on the course of the impact can be neglected as a whole.

Tab. 1. Mechanical properties of steel and copper

Properties	copper	steel
Longitudinal wave speed c_1 [m s^{-1}]	4597	5994
Shear wave speed c_2 [m s^{-1}]	2263	3204
Density ρ [kg m^{-3}]	8960	7830
Coefficient λ [GPa]	97.53	120.6
Shear modulus of elasticity G, μ [GPa]	45.9	80.4
Poisson number ν [-]	0.34	0.3
Young's module E [GPa]	123	209
Yield point R_y [MPa]	57	1000
Tensile strength R_m [MPa]	227	1200

Figures 2-5 show the time courses of the impactor characteristics during impact. It can be seen that, initially, the force acting on the impactor $P(t)$ during impact increases and reaches a maximum of P_{max} at t_{max}, $P_{max} = P(t_{max})$.
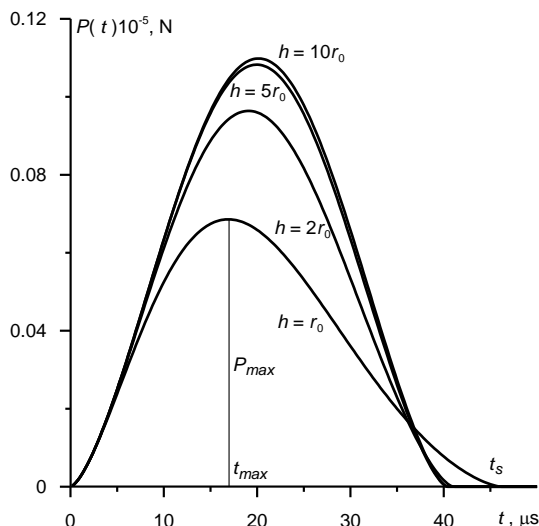
Fig. 2. Variation in impact force P over time for impact velocity V_0 = 10 m s^{-1}

A graph of the $P(t)$ relationship is shown in Figure 2 for different layer thicknesses. Impact velocity V_0=10 m s^{-1}. As the layer thickness increases, the values of P_{max} and t_{max} and for thickness h above 10 r_0 the layer can be regarded as a half-space. Time of

the event t_s decreases with increasing layer thickness, $P(t_s)$ = 0. In case of impactor collision with an elastic body t_{max} is less than half the impact time t_s. The sudden decrease of the impact force value observed in the figures is attributed to plasticity of the impact [40] and contact adhesion [41,42].

Figure 3 shows the change in impact force on the impactor P over time during a Hertz impact for an impact velocity of V_0=100 m s^{-1}. An increase in impact velocity leads to an increase in the maximum value of the interaction force P_{max} and reducing the impact time t_s and t_{max}. Qualitatively, the P runs have the same appearance. The quantitative values of the impact parameters are given in Tables 1 and 2 respectively for the impact velocity V_0=10 m s^{-1} and V_0=100 m s^{-1}.
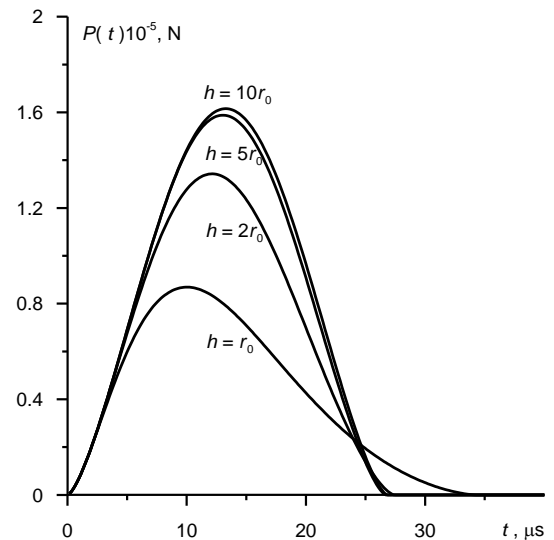
Fig. 3. Time variation of force on impactor P during Hertz impact for velocity V_0=100 m s^{-1}.
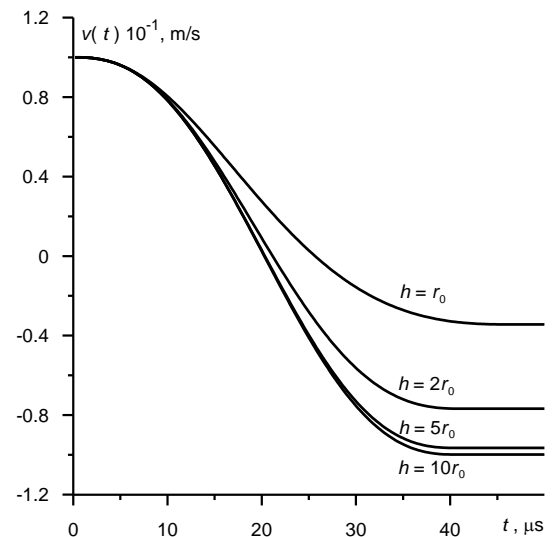
Fig. 4. Variation of the impactor velocity v in time during a Hertzian impact for the velocity V_0=10 m s^{-1}

Figures 4 and 5 show the velocity of the impactor $v(t)$ under impact with a layer of different thicknesses at different initial velocities. The velocity of the bumper decreases due to the force $P(t)$ to zero at a time greater than t_{max}, so it changes sign and reaches V_s=$v(t_s)$ at time t_s. The rebound velocity of the impactor will be used to calculate the coefficient of restitution R_f = V_s/V_0.

Yuriy Pyr'yev, Marek Pawlikowski, Rafał Drobnicki, Andrzej Penkul
Research of Dynamic Processes in a Layer During Collision with an Impactor

DOI 10.2478/ama-2024-0062

The numerical values of R_f are shown in Tables 2 and 3. This coefficient is the ratio of the velocity of the body after impact $v(t_s)$ to the velocity just before impact V_0. As the thickness of the layer increases, the rebound velocity V_s increases and for thickness h above 10 r_0 the rebound velocity equals the rebound velocity from the elastic half-space.
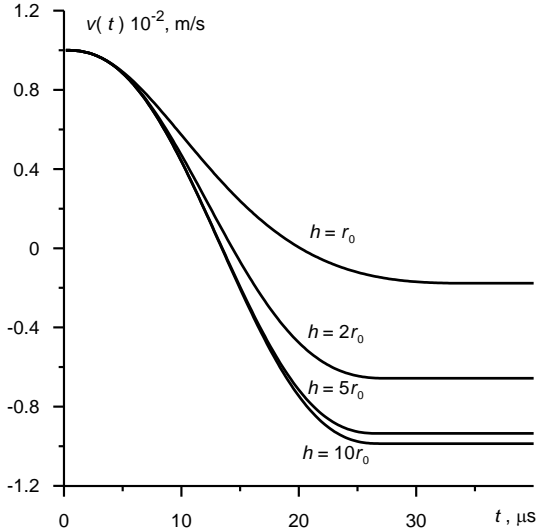
Fig. 5. Change of the impactor speed v in time during a Hertzian impact for the collision velocity V_0=100 m s^{-1}
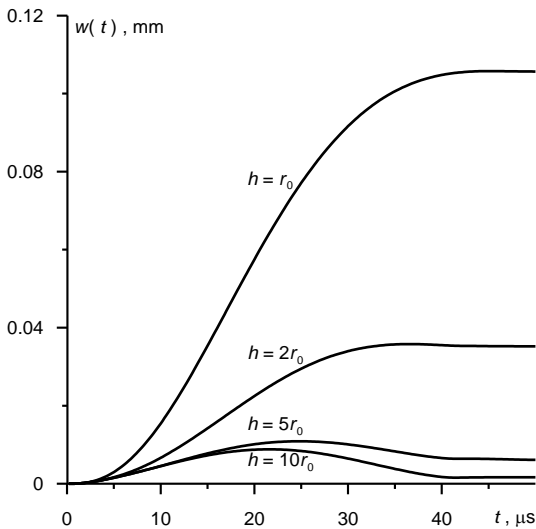
Fig. 6. Change of half-space deflection w in time during a Hertzian impact for the collision velocity V_0=10 m s^{-1}

In Figures 6 and 7 the displacement of the surface of the layer $w(t)$=$w(0,0,t)$ of different thickness during collision with the impactor at different initial speeds V_0 = 10 m s^{-1} and 100 m s^{-1} is shown. The displacement $w(t)$ for a small layer thickness ($h = r_0$) increases with time and reaches the greatest significance for $t = t_s$. Increasing the layer thickness causes the appearance of a maximum in the $w(t)$ relationship. An increase in the initial velocity causes an increase in the deflection of the layer at the collision point. Qualitatively, the deflections have the same appearance.

Numerical parameter values presented in Tables 2 and 3. Collision time t_s decreases with increasing layer thickness from 46 μs for thickness $h = r_0$ = 4 mm to 40.20 μs for thickness $h = 10 r_0$ (see the first row of Tab. 2). A tenfold increase in the collision

speed leads to the collision time t_s decreasing with increasing layer thickness from 34.30 μs to 26.72 μs (see the first row of Tab. 3). For such a speed, the duration of the collision t_s is too long to see the moments of arrival of the longitudinal P wave, transverse S wave and Rayleigh R wave. For a thickness $h = 5 r_0$, the time of collision with the layer does not differ from the time of collision with the elastic half-space.
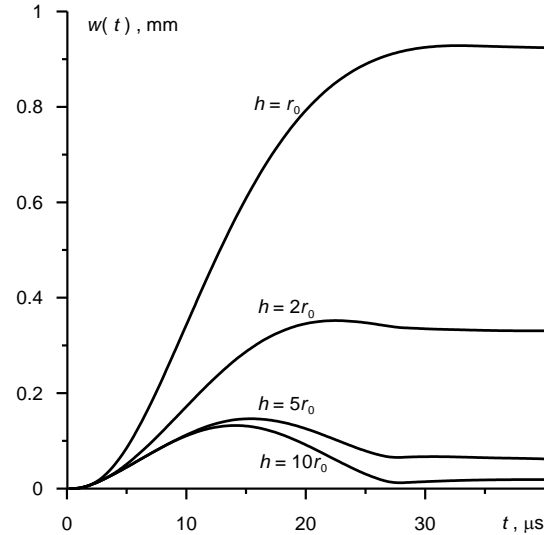
Fig. 7. Change of half-space deflection w in time during a Hertzian impact for collision velocity V_0=100 m s^{-1}

Tab. 2. Parameters of collision of the sample with a plate of thickness h for V_0 = 10 m s^{-1}

	$h = 1 r_0$	$h = 2 r_0$	$h = 5 r_0$	$h = 10 r_0$	$h = \infty$
t_s [μs]	46.00	41.00	40.20	40.20	40.4
t^*_s [μs]	46.5	40.8	39.8	39.6	40.8
t_{max} [μs]	17.00	19.00	20.00	20.02	20.02
t^*_{max} [μs]	16.7	19.00	19.65	19.5	19.65
P_{max} [kN]	6.856	9.639	10.83	10.98	11.00
P^*_{max} [kN]	6.812	9.7345	10.048	11.26	11.32
V_s=$v(t_s)$ [m s^{-1}]	3.44	7.68	9.65	9.98	10.0
$R_f = V_s/V_0$[-]	0.344	0.768	0.965	0.998	1.00
λ^* [-] (53)	0.6330	0.1582	0.025	0.0063	0.0016
R^*_f [-] (54)	0.3368	0.7618	0.9574	0.9892	0.9973
E_a [mJ]	538	250	42.0	2.44	0.00

Tab. 3. Parameters of collision of the sample with a plate of thickness h for V_0 = 100 m s^{-1}

	$h = 1 r_0$	$h = 2 r_0$	$h = 5 r_0$	$h = 10 r_0$	$h = \infty$
t_s [μs]	34.3	27.40	26.72	26.72	27.0
t^*_s [μs]	34.05	26.3	25.1	24.5	24.98
t_{max} [μs]	10.08	12.16	13.12	13.28	13.28
t^*_{max} [μs]	10.00	11.75	12.4	12.5	12.5
P_{max} [kN]	86.9	134.3	158.8	161.5	161.5
P^*_{max} [kN]	87.28	142.45	172.3	177.8	179.
V_s=$v(t_s)$ [ms^{-1}]	17.67	65.67	93.52	98.65	99.13
$R_f = V_s/V_0$[-]	0.177	0.657	0.935	0.986	0.991
λ^* [-] (53)	1.0032	0.2508	0.0401	0.0100	0.0025
R_f^* [-] (54)	0.1782	0.6498	0.9333	0.9829	0.9957
E_a [J]	59.1	34.7	7.65	1.64	1.06

Analysis of the numerical values of P_{max} indicates that there is an increase from 6.856 kN to 10.98 kN with increasing layer thickness for an impact velocity of 10 m s^{-1} and from 86.9 to 161.5 for V_0 = 100 m s^{-1}. We can also conclude that for layer thicknesses above h = 5 r_0, the maximum value of the impactor force P_{max} to the third significant digit does not differ from this value for the half-space.

The rebound velocity $V_s = v(t_s)$ increases from 3.44 m s^{-1} for layer thickness $h = r_0$ to 9.98 m s^{-1} for h = 10 r_0, initial velocity V_0 = 10 m s^{-1}. For the initial velocity V_0 = 100 m s^{-1}, the rebound velocity increases from V_s = 17.67 m s^{-1} for the layer $h = r_0$ to the value of 98.65 m s^{-1} for the layer with a thickness h = 10 r_0. Fig. 8 shows the values of the restitution coefficient $R_f = V_s/V_0$ as a function of the ratio of the layer thickness to the impactor diameter (h / r_0) for the impact speed V_0 = 10 m s^{-1} and V_0 = 100 m s^{-1}. As you can see from this figure, the coefficient of restitution increases and strive for the value of the coefficient of restitution for the elastic half-space.
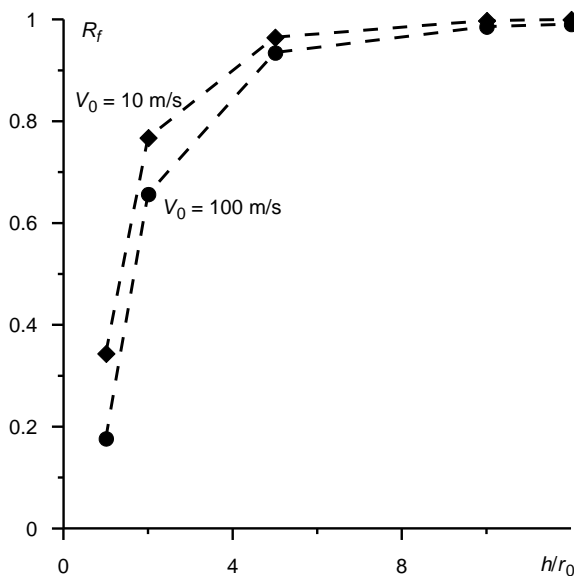
Fig. 8. Dependence of the coefficient of restitution R_f on the dimensionless parameter h / r_0 for collision velocities V_0=10 m s^{-1} and V_0=100 m s^{-1}

The last rows in Tables 2-3 present the absorption energy E_a. The conversion of kinetic energy is transformed into strain energy resulting from deformation

$$E_a = \frac{m_1 V_0^2}{2} - \frac{m_1 V_s^2}{2} \qquad (55)$$

Research has shown that thin layers have the best ability to absorb energy. The deformation energy at impact decreases as the collision speed increases.

Tables 2 and 3 show the corresponding kinematic and dynamic values (marked with an asterisk) calculated according to solving problem (49), (50) (Zener model [15]) taking into account (8), (47). Comparing the values without asterisks with the values with asterisks, we see that they come very close to a thin slab with thickness h = 2 h^*. This allows us to carry out the calculation of the impact parameters in a much simpler way.

Fig. 9, based on Tables 2 and 3, shows the results of the dependence of the coefficient of restitution R_f on the dimensionless parameter λ^* which is referred to in the literature as the inelasticity parameter[15]. Inelasticity is the dissipation of energy during a collision due to the formation of elastic waves which lift the energy away from the collision point.
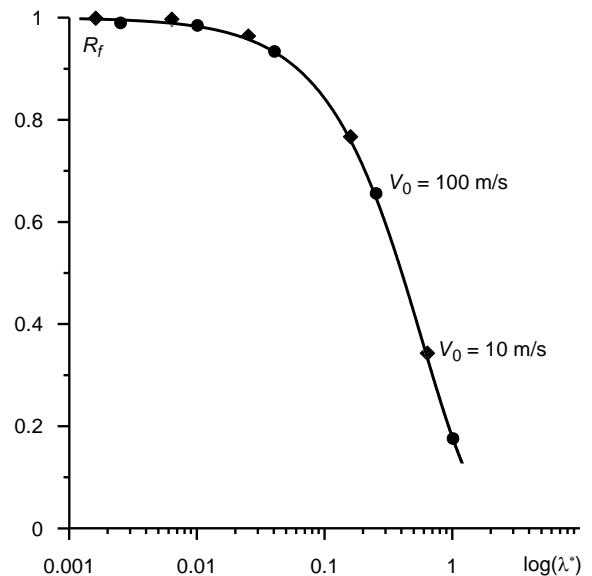
Fig. 9. Dependence of the coefficient of restitution R_f on inelasticity parameter λ^* for collision velocities V_0=10 m s^{-1} and V_0=100 m s^{-1}. Results from Tab. 2 presented in diamonds, results from Tab. 3 presented in circles, the solid line corresponds to formula (54) for R_f^*

For velocity V_0 = 10 m s^{-1}, the results are presented in diamonds and for V_0 = 100 m s^{-1} they are presented in circles. The solid line corresponds to the semi-empirical relationship (54) of the coefficient of restitution R_f^* with λ^*. The calculated results from the tables correlate well with this curve.

5. SUMMARY

A mathematical model of the dynamics of the contact system between a bumper and a layer of finite thickness during their collision has been developed. The proposed calculation method using classical Laplace and Hankel transforms allows to solve the problem of the spatial model of the body.

The proposed analysis makes it possible to calculate the stresses and displacements in the elastic layer, as well as the kinematics of the impactor.

Original elements of the paper include the proposed general approach to solving the contact dynamics problem. The approach presented is to determine the impact force on the sample $P(t)$ during impact as a joint solution of the problem for the impactor and the problem for the elastic layer under the assumptions of Hertzian theory. The resulting force $P(t)$ allows the determination of displacements and stresses.

The calculations carried out showed that for layer thicknesses of more than five impactor diameters, the layer can be considered as a half-space. The model of the anvil will be a half-space.

Let us point out that the Zener model [15] of the coefficient of restitution (54) for the elastic plate under the conditions considered agrees well with the results for the elastic layer including and for the half-space (Fig.9).

The proposed method can be useful for the dynamic analysis of issues such as the collision of a sample with a layered body [43].

sciendo

Yuriy Pyr'yev, Marek Pawlikowski, Rafał Drobnicki, Andrzej Penkul
Research of Dynamic Processes in a Layer During Collision with an Impactor

DOI 10.2478/ama-2024-0062

REFERENCES

1. Pyr'yev Y, Penkul A, Cybula L. Research of dynamic processes in an shield during a collision with a sample. Acta Mechanica et Automatica. 2023;6(3):77-87.
2. Taylor G. The use of flat-ended projectiles for determining dynamic yield stress. I. Theoretical considerations. Proc. R. Soc. London Ser. A. 1948;194:289–299.
3. Włodarczyk E, Michałowski M. Penetration of metallic half-space by a rigid bullet. Issues of Armament Technology. 2002;31(82):93–102.
4. Świerczewski M, Klasztorny M, Dziewulski P, Gotowicki P. Numerical modelling, simulation and validation of the SPS and PS systems under 6 kg TNT blast shock wave. Acta Mechanica et Automatica. 2012;6(3):77-87.
5. Kil'chevskii NA. Dynamic Contact Compression of Two Bodies. Impact [in Russian]. Kiev: Naukova Dumka; 1976.
6. Johnson KL. Contact mechanics. Cambridge: Cambridge University Press; 1985.
7. Kubenko VD. Impact of blunted bodies on a liquid or elastic medium. International Applied Mechanics. 2004;40(11):1185-1225.
8. Kubenko VD. Nonstationary deformation of an elastic layer with mixed boundary conditions. International Applied Mechanics, 2016; 52(6):563-580.
9. Ruta P, Szydło A. Drop-weight test based identification of elastic half-space model parameters. Journal of Sound and Vibration. 2005;282:411-427.
10. Achenbach JD. Wave propagation in elastic solids. North-Holland: Elsevier. 1973.
11. Senderowski C. Iron-aluminium inter metallic coatings synthesized by supersonic stream metallization. Warsaw: Bel Studio; 2015.
12. Miklowitz J. Transient Compressional Waves in an Infinite Elastic Plate or Elastic Layer Overlying a Rigid Half-Space. Journal of Applied Mechanics. 1962;29(1):53-60.
13. Valeš F, Šebkovà H. The state of stress in non-stationary loaded thin belt. Acta Technica ČSAV. 1976;4:439-458.
14. Kubenko VD, Salenko SD. Wave Formation in an Elastic Layer Under Moving Nonstationary Load. International Applied Mechanics. 2019;55(2):175-186.
15. Zener C. The intrinsic inelasticity of large plates. Physical Review. 1945;59(8):669-673.
16. Raman CV. On Some Applications of Hertz's Theory of Impact. Phys. Rev. 1920;15(4):277-284.
17. Peng Q, Liu X, Wei Y. Elastic impact of sphere on large plate. Journal of the Mechanics and Physics of Solids. 2021;156:104604.
18. Olsson R. Impact Response of Orthotropic Composite Laminates Predicted by a One-Parameter Differential Equation. AIAA Journal. 1992:30(6):1587-1596.
19. Smetankina NV, Shupikov AN, Sotrikhin SYu, Yareshchenko VG. A Noncanonically Shape Laminated Plate Subjected to Impact Loading: Theory and Experiment. J. Appl. Mech. 2008;75(5):051004.
20. Patil D, Higgs CF. A coefficient of restitution model for sphere–plate elastoplastic impact with flexural vibrations. Nonlinear Dynamics. 2017;88(3):1817-1832.
21. Mueller P, Boettcher R, Russell A, Truee M, Tomas J. A novel approach to evaluate the elastic impact of spheres on thin plates. Chem. Eng. Sci. 2015;138:689–697.
22. Muller P, Bottcher R, Russell A, True M, Aman S, Tomas J. Contact time at impact of spheres on large thin plates. Adv. Powder Technol. 2016;27:1233–1243.
23. Boettcher R, Russell A, Mueller P. Energy dissipation during impacts of spheres on plates: Investigation of developing elastic flexural waves. Int. J. Solids Struct. 2017;106:229–239.
24. Green I. The prediction of the coefficient of restitution between impacting spheres and finite thickness plates undergoing elastoplastic deformations and wave propagation. Nonlinear Dynamics. 2022; 109(4), 2443-2458.
25. Awrejcewicz J. Pyryev Yu. Nonsmooth Dynamics of Contacting Thermoelastic Bodies. New York: Springer Varlag; 2009.
26. Sears JE. On the longitudinal impact of metal rods with rounded ends. Proc. Cambridge Phil. Soc. 1908;14:257-286.
27. Hunter SC. Energy absorbed by elastic waves during impact. J. Mech. Phys. Solids. 1957;5:162-171.
28. Andersson M., Nilsson F. A perturbation method used for static contact and low velocity impact. Int. J. Impact Eng. 1995;16:759-775.
29. Timoshenko SP, Young DH, Weaver WJr. Vibration Problems in Engineering. New York: Wiley. 1974.
30. Argatov II. Asymptotic modeling of the impact of a spherical indenter on an elastic half-space. International Journal of Solids and Structures. 2008;45:5035-5048.
31. Rathore KK, Jasra Y, Saxena RK. Numerical simulation of fracture behavior under high-velocity impact for Aluminium alloy 6060 target plate. Materials Today Proceedings. 2020; 28(3):1809-1815.
32. Patra S, DasGupta A. Dependence of the coefficient of restitution on the shape of an impacting body. International Journal of Solids and Structures. 2023;281:112437.
33. Hertz H. Über die Berührung fester elastischer Körper [in German]. Journal für die reine und angewandte Mathematik. 1881;92:156-171.
34. Popov SN. Impact of a rigid ball onto the surface of an elastic half-space. Soviet Applied Mechanics. 1990;26(3):250-256.
35. Lamb H. On Waves in an Elastic Plate. Proceedings of the Royal Society. 1917; A, 93:114-128.
36. Awrejcewicz J, Pyryev Yu. The Saint-Venant principle and an impact load acting on an elastic half-space. Journal of Sound and Vibration. 2003;264(1):245-251.
37. Grinchenko VT, Meleshko VV. Harmonic vibrations and waves in elastic bodies [In Russian]. Kiev: Naukova Dumka; 1981.
38. Piessens R, Doncker-Kapenga ED, Überhuber CW, Kahaner DK. Quadpack. A Subroutine Package for Automatic Integration. Berlin Heidelberg: Springer-Verlag. 2011.
39. Argatov II. Fadin YA. Excitation of the Elastic Half-Space Surface by Normal Rebounding Impact of an Indenter. Journal of Friction and Wear. 2009;30(1):1-6.
40. Peng Q, Jin Y, Liu X, Wei YG. Effect of plasticity on the coefficient of restitution of an elastoplastic sphere impacting an elastic plate. Int. J. Solids Struct. 2021;222-223. 111036:1-11.
41. Ciavarella M, Joe J, Papangelo A, Barber JR. The role of adhesion in contact mechanics. J. R. Soc. Interface. 2019;16(151):20180738.
42. Peng B, Feng XQ, Li QY. Decohesion of a rigid flat punch from an elastic layer of finite thickness. J. Mech. Phys. Solids. 2020;139:103937.
43. Kulczycki-Żyhajło R, Kołodziejczyk W, Rogowski G. Selected issues of theory of elasticity for layered bodies. Acta Mechanica et Automatica. 2009;3(3):32-38.

Yuriy Pyr'yev: https://orcid.org/0000-0002-9824-2846

Marek Pawlikowski: https://orcid.org/0000-0002-3950-691X

Rafał Drobnicki: https://orcid.org/0000-0003-0582-5346

Andrzej Penkul: https://orcid.org/0000-0001-9855-6610